

Atmospheric circulation patterns that trigger heavy rainfall in West Africa

Jan Bliefernicht¹  | Manuel Rauch¹ | Patrick Laux^{1,2}  | Harald Kunstmann^{1,2} 

¹Institute of Geography, University of Augsburg, Augsburg, Germany

²Institute of Meteorology and Climate Research, Karlsruhe Institute of Technology, Garmisch-Partenkirchen, Germany

Correspondence

Harald Kunstmann, Institute of Meteorology and Climate Research, Karlsruhe Institute of Technology, Campus Alpin, 82467 Garmisch-Partenkirchen, Germany.
 Email: harald.kunstmann@kit.edu

Funding information

Bundesministerium für Bildung und Forschung, Grant/Award Numbers:
 01LG1202C1, 02WGR1421, 03SF0567D

Abstract

Classification of atmospheric circulation patterns (CP) is a common tool for downscaling rainfall, but it is rarely used for West Africa. In this study, a two-step classification procedure is proposed for this region, which is applied from 1989 to 2010 for the Sudan-Sahel zone (Central Burkina Faso) with a focus on heavy rainfall. The approach is based on a classification of large-scale atmospheric CPs (e.g., Saharan Heat Low) of the West African Monsoon using a fuzzy rule-based method to describe the seasonal rainfall variability. The wettest CPs are further classified using meso-scale monsoon patterns to better describe the daily rainfall variability during the monsoon period. A comprehensive predictor screening for the seasonal classification indicates that the best performing predictor variables (e.g., surface pressure, meridional moisture fluxes) are closely related to the main processes of the West African Monsoon. In the second classification step, the stream function at 700 hPa for identifying troughs and ridges of tropical waves shows the highest performance, providing an added value to the overall performance of the classification. Thus, the new approach can better distinguish between dry and wet CPs during the rainy season. Moreover, CPs are identified that are of high relevance for daily heavy rainfall in the study area. The two wettest patterns caused roughly half of the extremes on about 6.5% of days. Both wettest patterns are characterized by an intensified Saharan Heat Low and a cyclonic rotation near the study area, indicating a tropical wave trough. Since the classification can be used to condition other statistical approaches used in climate sciences and other disciplines, the presented classification approach opens many different applications for the West African Monsoon region.

KEY WORDS

circulation pattern, classification, downscaling, heavy rainfall, West Africa

1 | INTRODUCTION

West Africa is one of the poorest regions in the world, with an estimated total population of over 400 million

(UN, 2020). Monsoon rains are of utmost importance for this region, as the society is highly dependent on the production of rain-fed agriculture. The West African Monsoon (WAM) and its multi-scale atmospheric features

This is an open access article under the terms of the [Creative Commons Attribution](#) License, which permits use, distribution and reproduction in any medium, provided the original work is properly cited.

© 2022 The Authors. *International Journal of Climatology* published by John Wiley & Sons Ltd on behalf of Royal Meteorological Society.

have a significant impact on meteorological surface fluxes, such as precipitation at different spatiotemporal scales (e.g., Nicholson, 2001; Nicholson et al., 2018). Natural disasters, such as the Sahel drought in the 1970s and 1980s (Dai et al., 2004), the recent increase in flooding (Tazen et al., 2019), and related extremes (Salack et al., 2016; Taylor et al., 2017), have immediate and considerable macro-socioeconomic consequences for the West African nations (Markantonis et al., 2018). For instance, Munich RE (Munich, 2019) registered 82 drought events in West Africa with an estimated loss of more than US\$3.6 billion between 1980 and 2018. During the same period, 255 flood events were observed, causing over 200,000 inhabitants to become homeless (EM-DAT, 2020).

To reduce the negative impacts of such extremes, the hydro-meteorological services in West Africa need to provide reliable rainfall forecasts for different forecast horizons that can be used for decisions in agriculture and other disciplines. However, the current forecasting methods of the West African hydro-meteorological services are limited, as described, for example, by Bliefernicht et al. (2019) for seasonal forecasts. Moreover, state-of-the-art general circulation models (GCM) used in numerical weather prediction (NWP), or climate modelling do not provide accurate rainfall information at the local scale for West Africa. For instance, Vogel et al. (2018) showed that precipitation forecasts of nine global ensemble prediction systems were not able to outperform climatology-based forecasts, although sophisticated statistical postprocessing algorithms were applied. The study was done for three regions in northern tropical Africa using 1–5 day accumulated precipitation over a period of 7 years with a focus on point precipitation using common verification methods. In general, the capability of GCMs to simulate local rainfall is limited for many regions of the world, but their simulation for large-scale atmospheric circulation patterns (CPs) like the West African heat low or pressure systems over Europe provides much higher reliability (Smith et al., 2012). To overcome the GCM limitations, downscaling approaches are developed, ranging from dynamical (Giorgi and Gutowski, 2015) to statistical methods (Hewitson et al., 2014; Maraun and Widmann, 2018). Among the most common statistical downscaling techniques are classification approaches. These approaches classify the large-scale atmospheric circulation over a geographical region, to link this information to meteorological variables on the ground, such as rainfall or near-surface air temperature. Thus, a functional relationship is established between atmospheric variables (e.g., geopotential height) simulated by a GCM and locally observed meteorological variables on the ground. CP classification is of high interest for decision-making in water resources management and many other

disciplines (Bárdossy and Pegram, 2011). Hence, there is a multitude of approaches and applications (Huth et al., 2008; Philipp et al., 2016) which can be grouped into subjective, objective and mixed classification methods (Huth et al., 2008).

For the WAM region, very few studies have investigated the relationship between large-scale atmospheric features and meteorological variables with a CP classification on the local level. This type of technique is usually used and applied in mid-latitudes, where weather variability is mainly determined by the dynamics of high- and low-pressure systems. In contrast to mid-latitudes, weather variability in the WAM region is driven mostly by mesoscale convective systems (MCS), which can be related to African Easterly Waves (AEWs; Fink and Reiner, 2003; Moron et al., 2008a). AEWs impact day-to-day rainfall variability by facilitating the organization of MCSs. In addition, there is an increased probability of squall lines and rainfall in front of and in the trough of an AEW (e.g., Reed et al. 1977; Fink and Reiner, 2003). To identify and track AEWs, mid-tropospheric wind fields and their derived parameters, such as stream functions, are used (Berry et al., 2007; Brammer and Thorncroft, 2015). However, AEWs are not the only type of tropical wave that influences rainfall variability in this region. Schlueter et al. (2019a) and Schlueter, Fink and Knippertz (2019b) did a systematic comparison of six wave types and pointed out that Kelvin waves also play a role for daily rainfall variability on the local scale.

For the Western Sahel, Moron et al. (2008a) proposed an objective classification (k-means cluster analysis) of regional circulation, to analyse the influence of the circulation on local rainfall in Senegal. In this study, the clustering scheme was based on three wind levels (200, 700 and 925 hPa) for the period from July to September. The eight cluster-solution seems to be able to cover key features of daily circulation variability. Furthermore, the ability of GCMs to reproduce the mean seasonal cycle and transitions between CPs is strong, and the ability of GCMs to describe the interannual variability of CP occurrence, which affects the interannual variability of rainfall, is moderate to strong (Moron et al., 2008b). Guèye et al. (2011) identified nine CPs with self-organizing maps to account for the daily variability of atmospheric circulation over Senegal, using the mean sea level pressure and the wind field at 850 hPa as predictors. The CPs mainly show AEWs and the northward/southward displacement of the Saharan Heat Low (SHL). In the second part of the study, Guèye et al. (2012) investigated interannual variability and partly explained the interannual variation of summer rainfall over Senegal with their CPs. Laux (2009) linked the onset of the rainy season in the Volta basin of West Africa to large-scale atmospheric circulation patterns using a fuzzy rule-based classification

method. Camberlin et al. (2020) described six different types of intense rainfall events and their associated atmospheric circulation at the daily scale over southern West Africa. A common feature of all types is the existence of westward-propagating signals at the 700 hPa wind field. Moron et al. (2018) used a cluster analysis of daily pressure and wind anomalies to investigate to what extent CPs are relevant for intra-seasonal and interannual temperature variability in tropical North Africa.

The main objective of this study is the development of a statistical downscaling approach that relates atmospheric circulation patterns to heavy rainfall in the Sudan-Sahel region of West Africa. For this purpose, the fuzzy-rule based classification method (FRBCM) used by Laux (2009) for the onset of the rainy season is adapted and further advanced for daily precipitation extremes using a two-step procedure for the classification of daily CPs:

- First, a classification using large-scale atmospheric patterns (e.g., SHL) is performed to describe the strong seasonal rainfall variability in this region (hereinafter referred to as seasonal classification).
- Second, we further classified the wettest CPs from the seasonal classification to better describe the daily rainfall variability and heavy rainfall within the rainy season, by linking tropical wave features to regional rainfall (hereinafter referred to as subseasonal classification).

The FRBCM has been widely used for CP classification in different climate regions of the world (Wetterhall et al., 2006, 2008; Zehe et al., 2006a; Pringle et al., 2015). In this study, a two-step procedure for this classification approach for a climatologically challenging region is presented for the first time. The study builds on outcomes of specific WAM process studies (Diedhiou et al., 1998; Fink and Reiner, 2003; Berry et al., 2007; Engel et al., 2017) relevant for rainfall extremes to establish this downscaling approach for this region. Moreover, the two-step classification allows to incorporate additional predictor information like the stream function for describing ridges and troughs of tropical wave patterns over the study region. Since many classifications and other statistical downscaling studies carried out for this region were limited on certain monsoon periods (e.g., July–August–September), the novel approach applies a dynamic temporal domain based on atmospheric CPs for further refinement of the downscaling process. The study is supplemented by a comprehensive predictor screening and a sensitivity and transferability analysis of important parameters of the FRBCM, which has been not addressed in this level of detail by other investigations, so far.

2 | STUDY REGION AND DATA

2.1 | Target region and predictor domain

The study area is West Africa, specifically targeting (heavy) rainfall in Central Burkina Faso (Figure 1). This region belongs to the Sudan-Sahel zone, which is characterized by a strong seasonal rainfall variability (Laux et al., 2008; Laux et al., 2009; Bliefernicht et al., 2018). Table 1 shows that around 97% of the annual rainfall amount (741 mm/a) occurs from May to October and the period from May to September is most relevant for heavy rainfall in this region. In addition to the strong seasonal cycle, rainfall varies considerably during the rainy season. In this region, heavy precipitation is often the result of MCSs. This was shown, for instance, by Engel et al. (2017) for an extreme event in September 2009, which caused severe inundations in Ouagadougou, the largest city in Burkina Faso (Tazen et al., 2019).

To relate atmospheric patterns to rainfall within the study region, the CP classification is performed for two different domains. Domain A is used for the first step of the classification, that is, the seasonal classification, to describe the dominant large-scale seasonal features of the WAM processes, such as the SHL or the AEJ. It ranges from 30°W to 40°E and 5°S to 40°N and therefore covers most parts of Africa northward of the equator (Figure 1). The domain size is based on other downscaling studies done for West Africa (Dieng et al., 2018; Heinzel et al., 2018). Similar domains were also used by Lavaysse et al. (2009) for analysing the seasonal movement of the West African heat low and Nicholson (2013) for describing the WAM circulation. The second step of the classification, the subseasonal classification, applies domain B, ranging from 20°W to 20°E and 0°N to 20°N. Domain B is smaller than domain A, and better targets meso-scale synoptic features of tropical waves like AEWs. The choice of domain B was mainly based on Berry et al. (2007) who analysed a sequence of several strong AEWs for West Africa.

2.2 | Precipitation data

The daily rainfall data used in this study comes from a dataset established within the WASCAL (West African Science Service Centre on Climate Change and Adapted Land Use) project. A description of the rainfall dataset, with data sources and applied quality algorithms, is given in Bliefernicht et al., (2021). The rainfall dataset was also the source of information used in several other studies for this region, for example, for groundwater

reconstruction using hydrological models (Ascott et al., 2020) or validation of regional climate model simulations (Dieng et al., 2017). In this study, a subset of 26 stations was selected from the WASCAL database with daily data records from 1989 to 2010. The selected stations are in the middle of Burkina Faso and are therefore surrounding Ouagadougou (Figure 1b). The

mean data availability for this subset is relatively high (92.8%) with several almost complete time series (>99%) and 18 stations that contained more than 90% of the data records. The minimum data availability for a station in this subset was 72%. Two daily areal rainfall indices are computed from these subsets and are used as information for the development and evaluation of the classification approach:

- The daily areal rainfall probability (DARP) [–] is the number of wet stations divided by the total number of observations. A wet station is defined as a site with more than 1 mm/d rainfall.
- The daily areal rainfall amount (DARA) (mm/d) is based on the stations' average rainfall amount and is computed for each day as well.

2.3 | Reanalysis data

ERA-5 is the latest reanalysis dataset from the European Centre for Medium-Range Weather Forecasts and is used as predictor information. ERA-5 provides a detailed dataset of atmosphere, land and oceanic climate variables (Hersbach et al., 2020). ERA-5 replaced ERA-Interim (Dee et al., 2011) in 2019. Significant improvements compared with ERA-Interim are the temporal (hourly vs. 3-hourly) and spatial resolution (31 vs. 79 km), the number of vertical levels (137 vs. 60) and the increase of the amount of data assimilated, among many other issues (Hersbach et al., 2019). The ERA-5 data for the predictor screening was retrieved for each day of the investigation period (1989–2010) via the Climate Data Store of the Copernicus Climate Change Service. The ERA-5 information at 12 UTC was taken to preprocess the predictor information. 12 UTC was chosen as predictor time step due to former downscaling studies for daily precipitation extremes (Bifiefernicht, 2010), in which 12 and 18 UTC usually outperformed other 6-hourly time steps and daily averages.

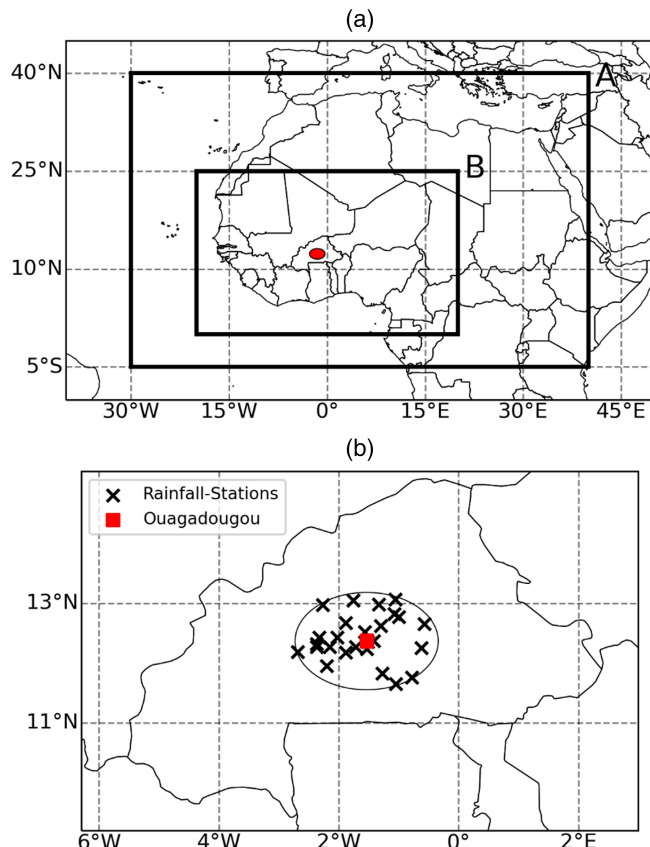


FIGURE 1 The upper panel shows domains A (30°W 5°S to 40°E 40°N) and B (20°W 0°N to 20°E 25°N) of the predictor variables used for the classification and the target region Central Burkina Faso (red ellipse). The lower panel shows a more detailed picture of the target region with the selected rainfall stations and the capital of Burkina Faso, Ouagadougou [Colour figure can be viewed at wileyonlinelibrary.com]

TABLE 1 Rainfall indices (RI) based on the daily areal rainfall amount for the study region

RI	Unit	Jan	Feb	Mar	Apr	May	Jun	Jul	Aug	Sep	Oct	Nov	Dec
P_m	(mm/m)	0.0	0.5	3.7	16.3	56.9	97.3	173.5	225.4	129.2	36.9	1.1	0.3
Q_{99}	(mm/d)	0.0	0.4	3.1	7.5	16.8	20.1	25.6	28.3	22.1	11.3	0.7	0.0
Max	(mm/d)	0.6	3.4	8.8	8.6	44.3	25.8	38.4	54.8	83.9	19.8	8.2	6.1
N_{ex}	(–)	0	0	0	0	5	7	26	46	15	1	0	0
P_1	(%)	0.1	0.7	1.8	5.4	14.2	21.2	31.7	39.5	28.6	10.4	0.9	0.5

Abbreviations: Max, maximum daily rainfall amount; N_{ex} , number of extremes; N_{ex} is based on the 100 largest daily events ($>19.6 \text{ mm/d}$); P_1 , rainfall probability (%), 1989–2010; P_m , mean monthly rainfall amount (mm/m); Q_{99} , 99%-quantile.

3 | METHODOLOGY

An overview of the dataflow and different components of the applied classification approach can be found in Figure 2. The core of the methodology is the fuzzy rule-based classification method (FRBCM), used for the classification of atmospheric CPs. The ERA-5 reanalysis and the WASCAL rainfall database provide the input for CP classification. First, a pool of predictor candidates for several atmospheric levels are tested for the classification and evaluated using an entropy-based information gain (Quinlan, 1986). Second, the predictor screening is supplemented by a sensitivity and transferability analysis, focusing on the number of CPs and number of grid points relevant for fuzzy rules. The different classification configurations are again evaluated using the information gain, and the best classification is chosen for further analysis.

The two-step procedure of our classification is implemented as follows. In the first step, the seasonal classification is performed to determine CPs that describe the large-scale circulation (e.g., SHL) over the study area. Since this classification is done for every day, a daily time series of CPs is generated for the investigation period. The seasonal classification is done for the predictor candidates listed in Table 2. The performance of the different predictor is evaluated how well the classification can discriminate between dry and wet days, and the best predictor candidate is selected. In the second step of the classification process, only the periods with wet CPs are chosen to perform the sub-classification. The subclassification is done using domain B and the predictor candidates of Table 2. Thus, the daily time series of the seasonal CPs are further refined based on the subseasonal classification.

The model development (classification) was done using reanalysis information provided by GCM which is very common for statistical downscaling (Brands et al., 2012; Maraun and Widmann, 2018). This makes it possible to evaluate the performance of a downscaling approach under “best” conditions (Brands et al., 2012). It has also the advantage that a direct functional relationship (without any time lag) between predictor (e.g., mean sea level pressure, stream function) and predictand (precipitation) can be established, in contrast to classical statistical forecasting (Wilks, 2011).

In the following, the different steps of the classification approach are explained in more detail.

3.1 | Fuzzy rule-based classification of circulation patterns

The fuzzy rule-based classification consists of three components: the calculation of anomalies for the selected predictor variable, the definition of fuzzy rules, and a simulated

annealing approach to optimize the functional relationship between predictor and predictand. For a detailed description of the fuzzy methodology, we refer to Bárdossy et al. (Bárdossy and Borgardi, 1995) and Bárdossy et al. (2002). The fuzzy classification has been applied by many other studies for different target variables and geographical regions of the world (Wetterhall et al., 2008; Pringle et al., 2015; Rau et al., 2020). In this study, a brief description of the different components is given.

For our application, it is assumed that the predictor variables are available in a regular grid at a daily resolution. The standardized anomalies $g(i,t)$ are calculated from the gridded predictor data $x(i,t)$ as:

$$g(i,t) = \frac{x(i,t) - \bar{x}(i)}{s(i)}, \quad (1)$$

where $i=1,\dots,I$ are the grid points, $t=1,\dots,T$ is the timestep in days, $\bar{x}(i)$ is the long-term mean and $s(i)$ is the long-term standard deviation over the entire time series.

Each CP is defined by a fuzzy rule. This implies that to each grid point i , membership functions are defined as triangular fuzzy numbers. Five different options for the degree of the anomaly at grid point i are considered: “very low”, “medium low”, “medium high”, “very high” and “indifferent.” The first four classes describe locations (grid points) with relevance to the CP, the fifth class indicates locations that have no influence on the classification. A CP with the fuzzy rule k is represented using the vector $v(k)=v(1,k),\dots,v(I,k)$, where $v(i,k)$ are the anomaly degree indices corresponding to grid point i for CP k . Membership function values are used in combination with the anomaly fields to compute the degree of fulfillment (DOF) for each CP (rule k). The rule with the highest DOF is assigned as CP for a given day.

The purpose of the optimization algorithm is to define fuzzy rules for each CP, for which the objective function $O(\vartheta)$ is maximum. As the objective function for the SA process, the following equation is used:

$$O(\vartheta) = \sqrt{\frac{1}{T} \sum_{t=1}^T (p(CP(t)) - \bar{p})^2}, \quad (2)$$

where T is the number of days, $p(CP(t))$ is the DARP exceeding the threshold ϑ within a given CP and \bar{p} is the mean DARP (exceeding threshold ϑ) without classification. For the threshold, $\vartheta=1 \text{ mm/d}$ is used. A detailed description of the simulated annealing algorithm is also given in Appendix A.

A relevant model parameter of the classification approach is the number of CPs, as shown by Bárdossy (2010) and Pringle et al. (2015). In addition, the

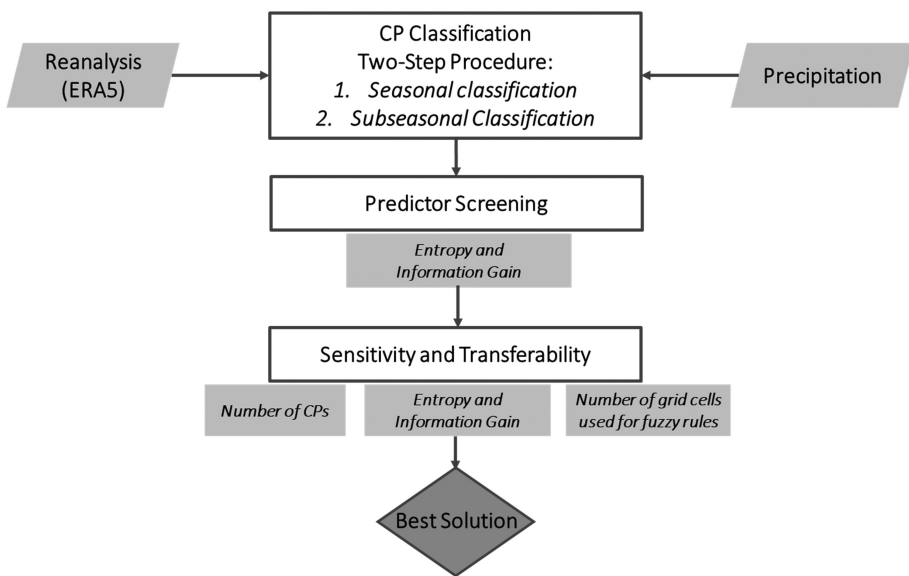


FIGURE 2 Flowchart of the classification approach followed in this study to determine atmospheric circulation patterns (CP)

TABLE 2 List of predictor variables used for the seasonal (domain A) and subseasonal classification (domain B, see Figure 1 for the domains)

Variable	Abbreviations	Pressure levels (hPa)	Classification	Study
Geopotential height	GPH	200, 500, 700, 850, 1000	Seasonal	b
Temperature	TEMP	1000	Seasonal	b
Zonal wind	U	200, 500, 700, 850, 1000	Seasonal	a,b,d,e
Meridional wind	V	200, 500, 700, 850, 1000	Seasonal	a,b,c,d,e
Specific humidity	SH	850, 1000	Seasonal	–
10 m zonal wind	10 mU	–	Seasonal	–
10 m merid. wind	10 mV	–	Seasonal	–
2 m air temperature	2 mT	–	Seasonal	–
Mean s.l. pressure	MSL	–	Seasonal	b, c, d
Zonal moisture flux	MFU	850, 1000	Seasonal	b
Merid. moisture flux	MFV	850, 1000	Seasonal	b
Stream function	SF	700, 850	Subseasonal	–
Relative vorticity	RV	700	Subseasonal	–
Curvature vorticity	CV	700	Subseasonal	–
Shear vorticity	SV	700	Subseasonal	–
Zonal wind	U	700	Subseasonal	–
Meridional wind	V	700	Subseasonal	–

Note: a, Moron et al. (2008a); b, Laux (2009); c, Guèye et al. (2011); d, Moron et al. (2018); e, Camberlin et al. (2020).

Abbreviations: merid., meridional; s.l., sea level.

number of grid points relevant for the fuzzy rules (ANC) plays an important role for the classification. Thus, at these grid points, one of the four fuzzy rules “very low”, “medium low”, “medium high” and “very high” is assigned by the algorithm. By changing both parameters, an optimal number of CPs and ANC value can be determined for the classification.

3.2 | Performance measures

The basis of the performance measures used in this study is the entropy E, proposed by Shannon (1948):

$$E = - \sum_{i=1}^n p_i \log_2 p_i, \quad (3)$$

where p_i is the rainfall frequency for n rainfall categories. A rainfall data set containing only the same values has a very low (zero) entropy, whereas a data set with very different rainfall values has a relatively high entropy. The Shannon entropy is widely used in many different disciplines and has been also used for CP classification (Pringle et al., 2015).

The entropy function is used to compute the corresponding information gain IG (Quinlan, 1986; Li and Claramunt, 2006):

$$IG = E - \sum_{k=1}^K f_k E_k, \quad (4)$$

where K is the number of CPs, f_k is the relative CP frequency and E_k the entropy of each CP. IG indicates how much entropy is removed when the data set is partitioned into several subsets (in our case the different CPs). In other words, the higher IG is, the more entropy is eliminated, and the better the CP classification can distinguish between wet and dry CPs. The precipitation threshold for the computation of the information gain is 1 mm/d for the seasonal and 5 mm/d for the subseasonal classification.

For the analysis of the CP-dependent rainfall conditions (e.g., wet and dry), the mean daily areal rainfall probability (MDARP) and the mean daily areal precipitation amount (MDARA) is calculated. In addition, the wetness index (WI) for each CP is computed Bárdossy (2010). WI [–] is defined as the ratio of the conditional MDARA of a CP to the unconditional MDARA (average DARA) for the studied period. A WI value greater (smaller) than 1 implies that the CP is wetter (drier) compared with the climatological mean.

3.3 | Predictor screening

Regardless of the chosen CP classification method, the relevance of the obtained CPs depends on the selected predictors. Suitable predictor variables should be able to describe the main atmospheric characteristics of the study region. Over West Africa, seasonal and daily rainfall variability is constituted by complex interactions of different WAM processes (Nicholson, 2013). Thus, a comprehensive predictor screening is done to determine the most suitable predictor variables for both classification steps. To achieve this task, the ERA5 reanalysis fields were preprocessed with bilinear remapping from $0.25^\circ \times 0.25^\circ$ to $2^\circ \times 2^\circ$ resolution for the predictor screening. This is a common method to save computational effort in FRBCM, especially for variables like mean sea-level pressure, which have a low spatial heterogeneity.

The list of potential predictor variables selected from ERA-5 used for the classification can be found in Table 2. In addition to variables directly provided by ERA5, the zonal and meridional moisture flux component was calculated. These variables were previously chosen for downscaling daily precipitation, for example, by Bliefernicht and Bárdossy (2007) for Central Europe and Laux (2009) for West Africa. The choice of predictor variables for domain A was mainly based on previous classification studies done for this region (see the references in Table 2). However, we included further variables like temperature and additional pressure levels (e.g., 500 hPa). For the subseasonal classification we used several vorticity parameters, wind components and the stream function at the 700 and 850 hPa level (Li et al., 2006; Berry et al., 2007). Based on the stream function field, the rotational flow can be determined to determine troughs and ridges of AEWs (Berry et al., 2007).

Potential predictor variables of the seasonal classification are analysed for their performance in discriminating between rainy and dry season. For this classification, the FRBCM is performed for domain A using 10 CPs and an ANC of 100 in the SA process. The subseasonal classification is only done for the wettest CPs of the seasonal classification. Six CPs and an ANC of 10 in the SA process are used for the predictor screening.

3.4 | Sensitivity and transferability analysis

The transferability of a classification to an independent data set is a basic requirement for the development of a reliable downscaling approach. To address this issue, FRBCM is trained and validated using a split-sampling approach. The training dataset ranges from 2000 to 2010 and is used for optimization of FRBCM. Afterwards, the optimized rules are transferred to the validation period of 1989 to 1999. Since the performance of the fuzzy approach depends on different parameters, like the number of CPs and the number of grid points relevant for fuzzy rules (ANC), we perform an analysis on both parameters to determine an optimal classification for the target region in terms of model performance and transferability. Only the number of CPs was addressed in previous investigations (Bárdossy, 2010; Pringle et al., 2015), so far.

Since ANC has a strong influence on the transferability of the FRBCM, the parameter is decreased from 207 (25% of the grid-points) to 16 (2% of the grid points) in domain A. This investigation is done using MSL because this variable scored best among the selected variables in the first predictor screening. The same analysis is

done for SF700 on domain B using 18, 10 and 5 grid points. An analysis on how the number of CPs affects the information gain for both classifications is also performed. 6 to 12 classes are used for the seasonal classification, and 4 to 8 classes for the subseasonal classification. A higher number of classes is not used to determine CPs with appropriate sample size for the final classification.

4 | RESULTS

In the following, the results of the seasonal and the subseasonal classification are presented. For both classifications, a predictor screening is performed first, followed by the analysis of the sensitivity and transferability of the classification approach. In addition, the identified circulation patterns and their wetness is analysed for both classifications. The purpose of this analysis is to describe whether physically reliable atmospheric circulation patterns can be obtained by the classification process, rather than mathematical artefacts (Wetterhall et al., 2007). This is an important step in objective classification and was also done by many other FRBCM studies (Zehe et al., 2006a; Wetterhall et al., 2008; Pringle et al., 2015). Finally, an evaluation of the two-step classification procedure for heavy rainfall is presented.

4.1 | Seasonal classification

In this section, the outcomes (predictor screening, sensitivity and transferability analysis, circulation patterns) of the seasonal classification (domain A, see Figure 1a) are described in detail.

4.1.1 | Predictor screening

Figure 3 shows the performance of the candidates used for the predictor screening of the seasonal classification. The near-surface temperature variables T2M and TEMP1000, which indicate the temperature contrast between the Tropical Atlantic and West Africa, perform best ($IG = 0.42$) in describing the rainfall seasonality. A slightly lower performance is obtained for MSL ($IG = 0.41$) and GPH1000 ($IG = 0.40$). Both variables can be seen as an indicator for the SHL. Very similar results are obtained for the near-surface wind components U1000 ($IG = 0.40$) and V1000 ($IG = 0.39$), as well as the near-surface meridional moisture flux MFV1000 ($IG = 0.38$). These predictors are closely related to the Southwest Monsoon and the Harmattan. Moreover, the zonal wind fields at 700 hPa (U700) and

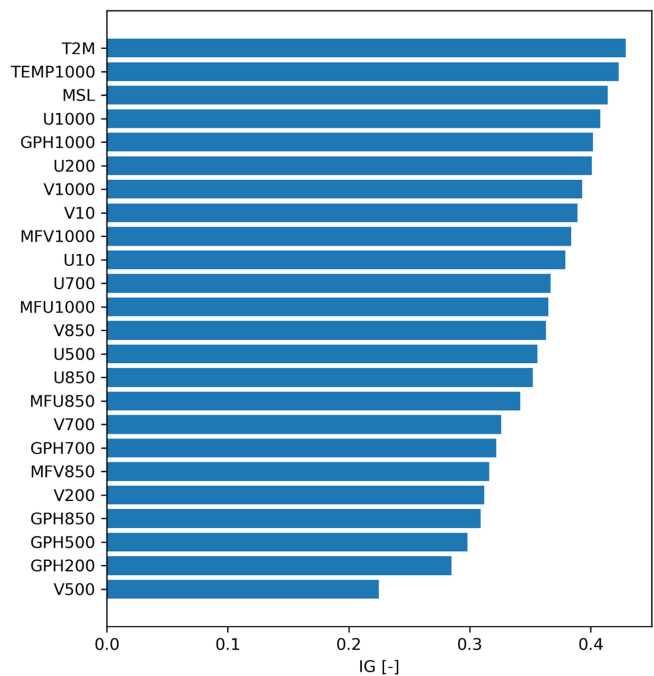


FIGURE 3 Predictor screening for the seasonal classification. Results are shown for the calibration period (2000–2010) and sorted from high to low information gain (IG) values. T2M and MSL are therefore the best predictors with the highest information gain. The abbreviations of the predictors are explained in Table 2 [Colour figure can be viewed at wileyonlinelibrary.com]

200 hPa (U200), representative of the African Easterly Jet and the Tropical Easterly Jet, respectively, also have a relatively high information gain ($IG > 0.37$). They outperform other predictors such as V200, V700 and U850, which cannot be related to large-scale seasonal WAM processes. This gives sufficient credibility that the predictor screening reflects major governing WAM processes quite well.

The significance of the outcome of the predictor screening was also analysed using a bootstrap method (Efron and Tibshirani, 1994; Chernick, 2011). The basis is an algorithm presented in Bliefernicht et al. (2019), which was slightly adapted for the calculation of the information gain and for performing a pairwise test of the performance differences for each predictor pair. Figure 4 shows that the differences are only non-significant for predictor pairs with very similar model performances (e.g., T2M and MSL or MSL and U1000). Thus, for most of the tested predictor pairs (88.6%) the differences in model performance are significant.

Ultimately, the predictor variables U1000, V1000, MSL, GPH1000, U700, U200 and MFV1000 are selected by the predictor screening and used for further analysis. Similar predictors of the selected variables like U10 or V10 are no longer considered. The same also applies for near-surface temperature variables like T2M and

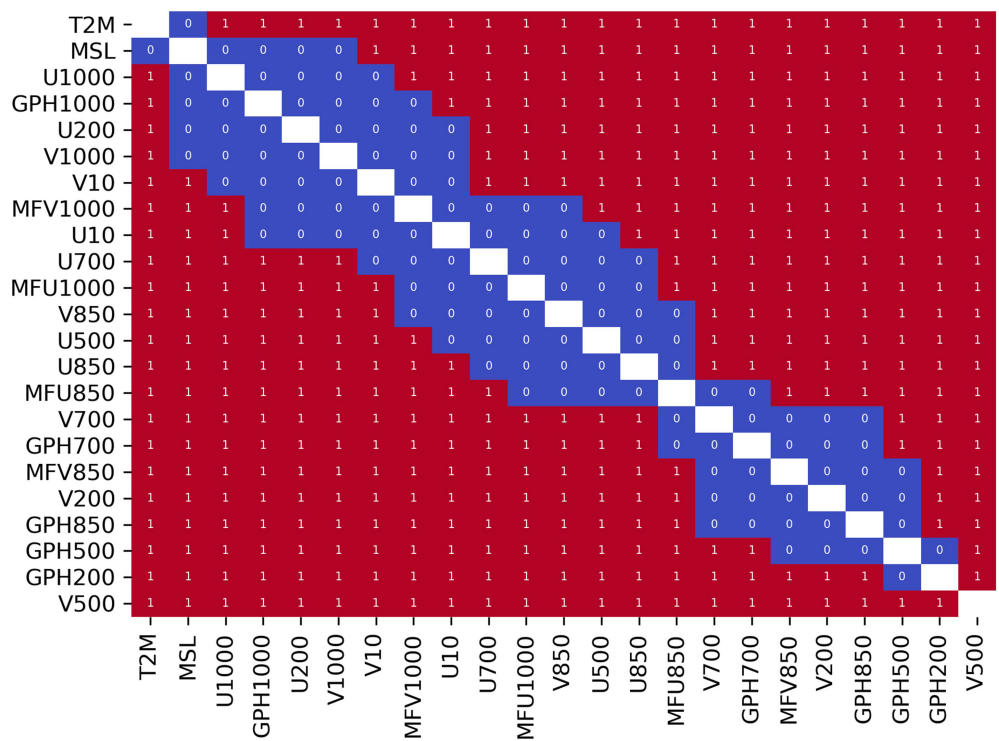


FIGURE 4 Significance of the results of the predictor screening shown in Figure 3. The significance of the performance differences between two classifications with different predictors (e.g., MSL and U1000) was tested for each pair using a bootstrap analysis on a significance level of 5%. Red indicates a statistically significant difference in performance between two classifications (1), whereas blue indicates no significance (0). For instance, row 1 indicates that a classification using T2M was superior compared with all other classifications except a classification using MSL. The abbreviations of the predictors are explained in Table 2 [Colour figure can be viewed at wileyonlinelibrary.com]

TEMP1000, since these are closely related to MSL and GPH.

4.1.2 | Sensitivity and transferability

The results of the transferability analysis are exemplarily shown in Figure 5 for the seasonal classification and MSL as the predictor variable. The performance of the classification in the calibration period is best for the highest ANC values ($IG = 0.41$ with 207 ANC) and tends to decrease with smaller ANC values ($IG = 0.36$ with 16 ANC, Figure 5). However, the information gain of the validation increases with a decreasing ANC and reaches its optimum at 55 ($IG = 0.29$). Thus, only a small fraction of grid points should be used for the training of fuzzy rules, otherwise, if the established fuzzy rules are transferred to the validation set, approx. 40% of performance in terms of the information gain is lost. Since the transferability and the performance is highest for $ANC = 33$ (corresponding to a fraction of 0.04% of grid points used for the fuzzy rules), this value is used in the following.

Respectively, the FRBCM is performed for the chosen predictor variables (U1000, V1000, MSL, U700, U200, V850, MFV1000 and GPH1000) in Domain A with 33 ANC in the SA process and 10 CPs. In comparison to the results of Section 4.1.1, all predictor variables suffer performance losses during the calibration period because of a reduced ANC (Figure 6). However, almost all variables (except for U1000) show an improvement in the validation period. This confirms our assumption that by reducing ANC, the transferability of the classification can be improved to a certain degree. Interestingly, the ranking of the best predictors is slightly changed. In this case, MFV1000 performs best, followed by MSL and U200. Thus, this indicates that it is necessary to perform a detailed analysis for every predictor variable, that is, to determine an optimal number of grid points. MSL and MFV1000, the two most performant variables, are used exemplarily to study the impact of the number of CPs (6, 8, 10 and 12) on the information gain (see Figure 7).

The outcomes of this analysis show that the number of CPs also has a considerable impact on the performance of the classification. The highest performance is achieved if 8 to 10 classes are selected for MSL, and 10 to 12 classes

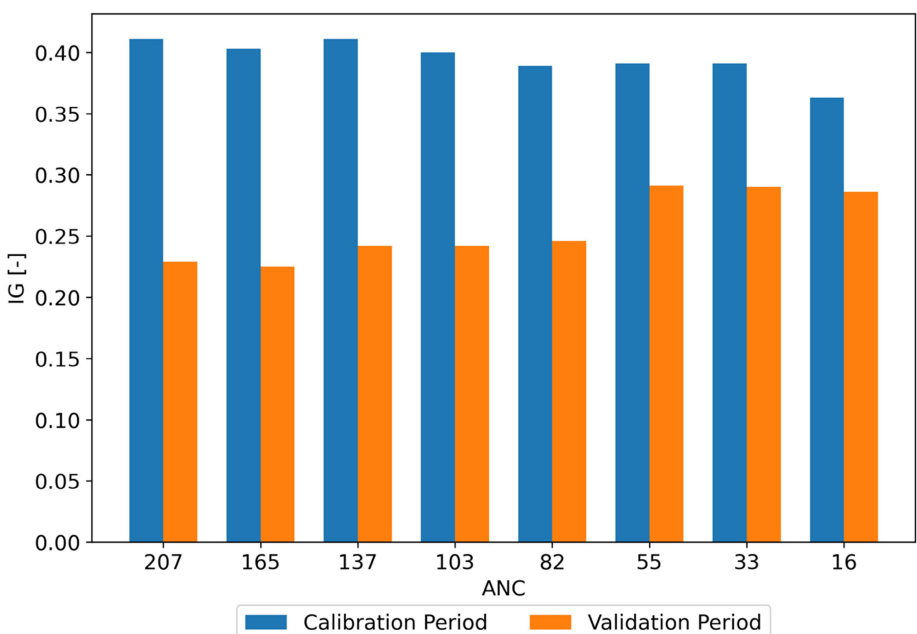


FIGURE 5 Performance of the seasonal classification for the calibration and validation period using different numbers of grid points (ANC) in the fuzzy rules and mean sea level pressure as predictor variable. IG, information gain [Colour figure can be viewed at wileyonlinelibrary.com]

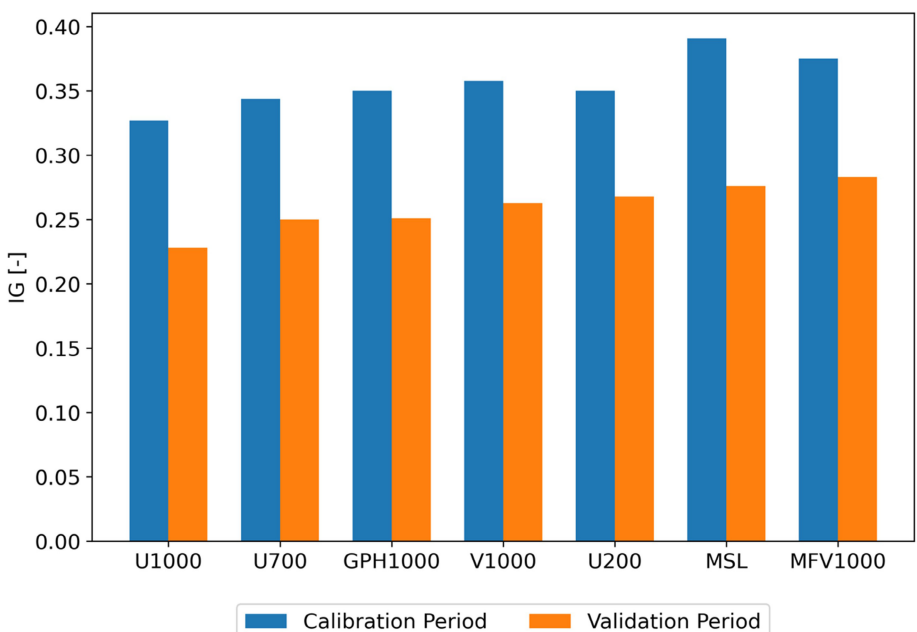


FIGURE 6 The performance of the seasonal classification for different predictors using 33 grid points in the fuzzy rules (ANC = 33). The variables on the x-axis are sorted by the information gain (IG) in the validation period. The predictor abbreviations are explained in Table 2 [Colour figure can be viewed at wileyonlinelibrary.com]

for MFV1000. The MSL classification using eight CPs shows the highest performance and is therefore used as the best solution for the seasonal classification.

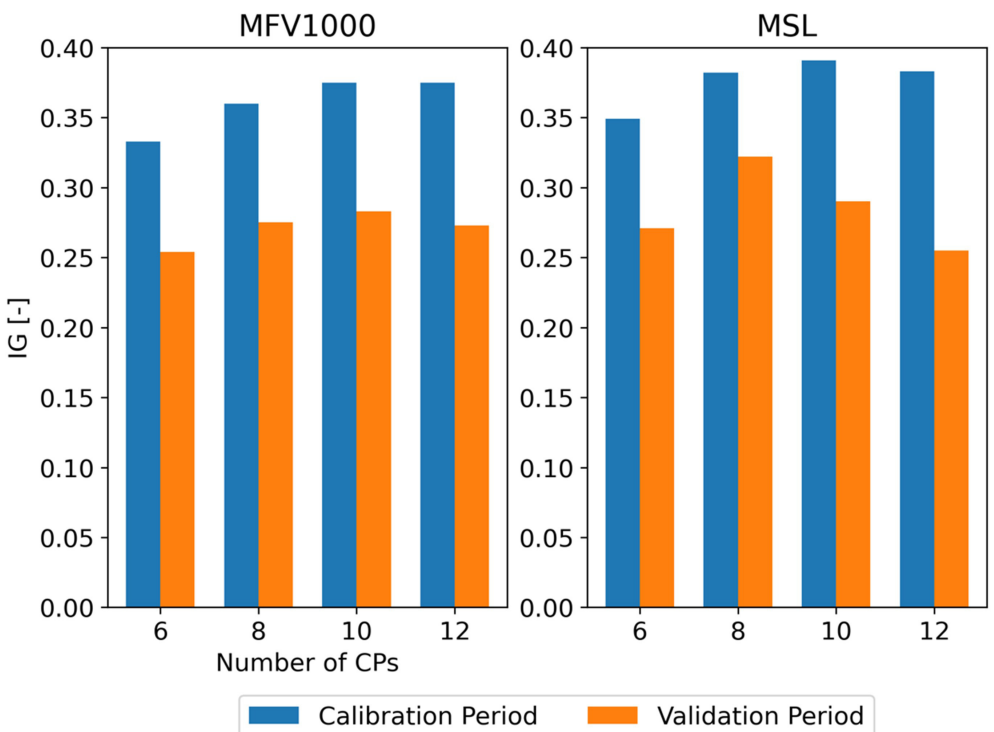
4.1.3 | Description of circulations patterns

Figure 8 shows the spatial CP patterns of the MSL anomalies from the seasonal classification. An important feature of the MSL fields is the negative pressure anomalies indicating the West African heat low. This heat low exists throughout the year and occurs where insolation is high,

and evaporation is low. It shifts northwest from its winter position (November–March, CP7) by the Darfur Mountains to its summer position (June–September) between the Hoggar and the Atlas Mountains above the Sahara, known as the SHL (CP2, CP4, CP5, Lavaysse et al., 2009).

During the dry phase (November to March) of the WAM, CP1, CP6 and CP7 are predominant (Tables 3 and 4). In general, these patterns have quite a similar structure with a high surface pressure (i.e., positive anomalies) in the north and low surface pressure (i.e., negative anomalies) in the south. CP6 is most characteristic for the dry phase, while CP1 and CP7 can also appear in

FIGURE 7 The performance of seasonal classification for meridional moisture fluxes at 1000 hPa level (MFV1000) and mean sea level pressure (MSL) with respect to the number of CPs [Colour figure can be viewed at wileyonlinelibrary.com]



April and May during the WAM transition phase. The MDARP (WI) remains below 0.04 (0.19) for CP1, CP6 and CP7, indicating that these CPs are extremely dry.

During the transition phase of the WAM (April, May, October) CP2, CP3 and CP8 operate as a kind of bridge to the other phases. There is a northward (southward) progression between 10 and 20°N of the West African heat low (CP3, CP8), with a zonal expansion (reduction) related to the seasonally varying solar insolation following the zenith position of the sun. As the seasonal cycle progresses, the zonal expansion of the heat low decreases and changes to the state in CP2, where the SHL between the Hoggar and the Atlas Mountains starts to intensify as a precursor for the summer phase. During the transitional phase, the southwest monsoon is shifted inland, initiating the rainy season in the study region. In consequence, CP2, CP3, CP8 are relatively wet in comparison to the CPs of the dry phase.

During the WAM main phase (June to September), CP2, CP4 and CP5 are the prevailing patterns. CP2 occurs as pre- and post-monsoonal pattern in June and September, in addition to CP4 and CP5 in July and August. In comparison to CP2, the core of the SHL in CP4 and CP5 is much stronger, and a north-west migration can be observed. The southwest monsoon flow is strongest and the ITCZ/ITD reaches its northernmost position. Thus, CP2, CP4 and CP5 are the wettest CPs for the study region and explain approx. 87% of the total areal precipitation amount of the study region.

4.2 | Subseasonal classification

In this section, the outcomes (predictor screening, transferability and sensitivity analysis and circulation patterns) of the subseasonal classification (domain B) are presented.

4.2.1 | Predictor screening

The outcomes of the predictor screening for the subseasonal classification are shown in Figure 9. The relative vorticity RV700 has the highest performance ($IG = 0.07$) for the calibration period, followed by the stream functions SF700 and SF850. Note that the scale is an order of magnitude smaller compared with Figure 6. Slightly lower IGs (0.05) are achieved for the calibration period by the other predictors. However, many predictors are considerably weaker for the validation period. Several predictors, like the zonal wind component, tend to zero information gain. The only predictor with similar performance for the validation period is the stream function at the 700 hPa level. Thus, this predictor allows a much better transferability of the classification approach and has the highest overall model performance for both periods. It is therefore chosen for further analysis. The performance loss for the validation period of the wind and vorticity predictors can be partly explained by their strong spatial heterogeneity. The stream functions only include the rotational component and no divergence, and therefore have a much smoother spatial field compared with the vorticity parameters.

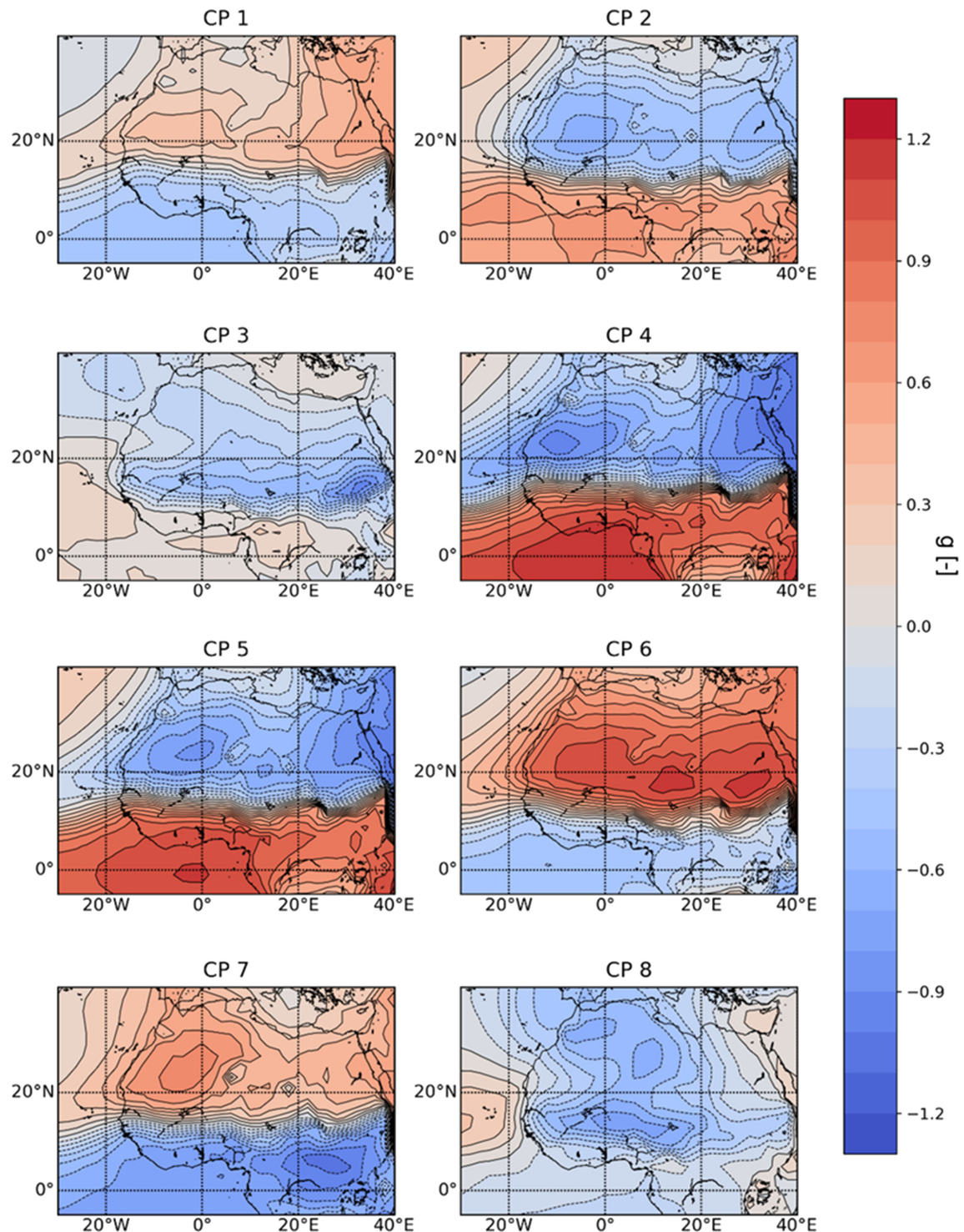


FIGURE 8 Atmospheric circulation patterns (CP) of the seasonal classification using mean sea level pressure anomalies (1989–2010) within domain A [Colour figure can be viewed at wileyonlinelibrary.com]

4.2.2 | Sensitivity and transferability

Several findings of the transferability and sensitivity analysis in Section 4.1.2 are confirmed by the subseasonal classification using SF700 (Figure 10, left). A

classification setting with 10 ANC, and therefore 4% of the grid points, has the highest performance in the validation period. In addition, performance increases with a higher ANC for the calibration period but decreases for the validation period. Investigating the impact of the

TABLE 3 Circulation pattern (CP) statistics (1989 to 2010) for the seasonal classification using mean sea level pressure and for domain A

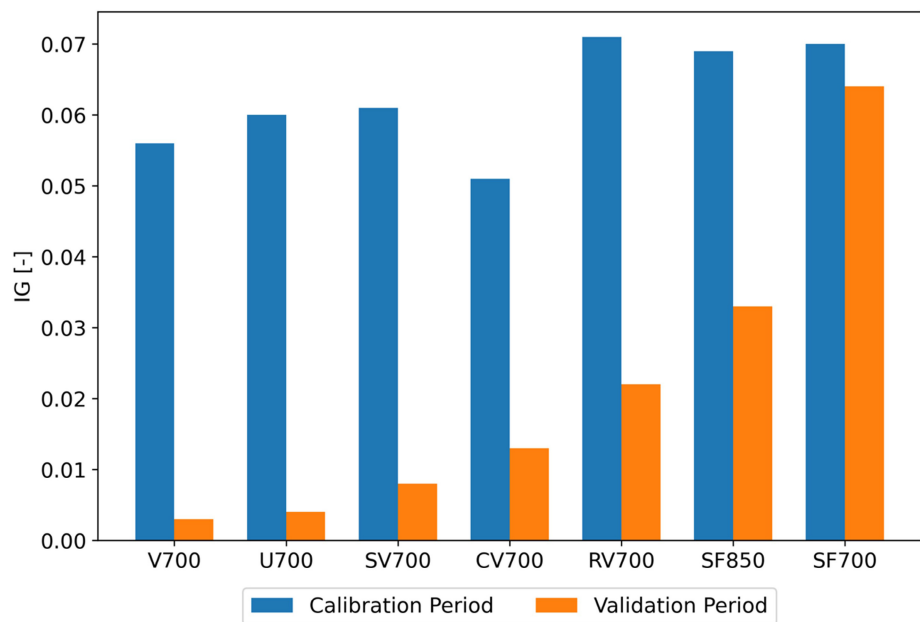
CP	Occurrence (%)	MDARP (-)	MDARA (mm/d)	WI (-)
1	13.37	0.04	0.39	0.19
2	7.44	0.21	3.07	1.51
3	7.37	0.09	1.15	0.57
4	14.00	0.36	6.62	3.26
5	13.90	0.28	4.42	2.18
6	22.39	0.01	0.07	0.04
7	13.14	0.01	0.07	0.04
8	8.39	0.09	1.16	0.57

Abbreviations: MDARP, mean daily areal rainfall probability; MDARS, mean daily areal rainfall amount; WI, wetness index.

TABLE 4 Monthly occurrence frequencies (%) for each circulation pattern (CP) of the seasonal classification using mean sea level pressure within domain A

Month	CP1	CP2	CP3	CP4	CP5	CP6	CP7	CP8
Jan	16.9	0.0	0.4	0.0	0.0	53.5	28.0	1.2
Feb	17.4	0.3	1.3	0.0	0.0	47.2	30.1	3.7
Mar	21.8	1.5	4.0	0.1	0.0	28.2	32.0	12.5
Apr	30.2	5.2	11.8	0.5	0.8	8.8	16.2	26.7
May	13.9	18.9	23.3	2.3	10.1	3.4	3.1	24.9
Jun	1.2	22.3	9.1	17.4	44.2	0.3	0.0	5.5
Jul	0.4	9.2	0.7	47.1	40.9	0.0	0.0	1.6
Aug	0.0	4.4	0.3	59.2	34.5	0.0	0.0	1.6
Sep	3.8	13.8	6.4	37.3	32.3	1.4	0.6	4.5
Oct	17.7	12.3	26.5	2.8	3.5	13.6	8.2	15.2
Nov	22.0	0.6	3.8	0.0	0.0	53.8	17.7	2.1
Dec	15.5	0.6	0.3	0.0	0.0	60.0	22.7	0.9

FIGURE 9 Predictor screening for the subseasonal classification, using the information gain (IG) sorted from low to high values of the validation period. The abbreviations of the predictors are explained in Table 2 [Colour figure can be viewed at wileyonlinelibrary.com]



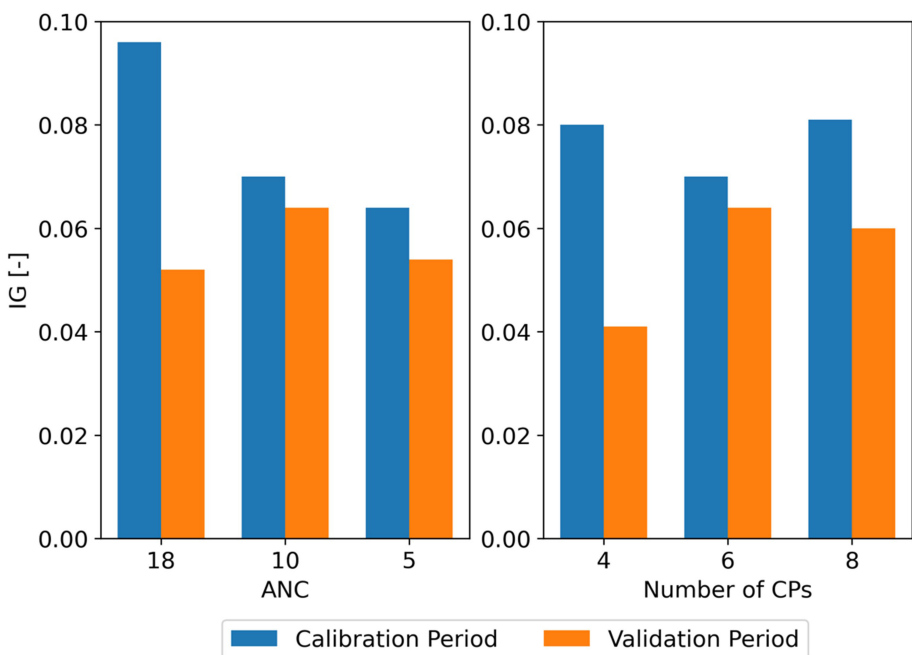


FIGURE 10 The performance of the subseasonal classification for the calibration and validation period using the stream function at 700 hPa level for several configurations with respect to the grid points in the fuzzy rules (ANC) and to the number of circulation patterns (CP) [Colour figure can be viewed at wileyonlinelibrary.com]

number of CPs on the information gain (Figure 10, right) reveals that SF700 with six classes performs best, with slight tendencies to higher information loss of the optimized classification for the validation period if four or eight subgroups are selected. Thus, the classification using SF700 with 10 ANC and six subgroups is selected as the best solution for the subseasonal classification.

4.2.3 | Description of circulation patterns

The six atmospheric CPs for the best subseasonal classification using SF700 are shown in Figure 11. The negative (positive) anomalies of SF700 indicate cyclonic (anticyclonic) circulations over the study region. For instance, CP1 and CP2 show strong positive anomalies over the study region, indicating that this area is influenced by anticyclonic circulations and resulting in drier conditions ($WI < 0.7$, Table 5). In turn, CP4 and CP6 are characterized by strong negative anomalies, leading to much wetter conditions ($WI > 1.5$). For instance, MDARA of the wettest pattern (CP4) has a value of 8.27 mm/d, which is nearly three times larger compared with **driest pattern** (2.85 mm/d, CP2). Moreover, the results of this analysis also indicate that the location of the negative anomalies plays a role. The negative anomaly of CP4 and CP6 is much closer to the study region in comparison to the drier CP5. Thus, the results of this analysis suggest that the subseasonal classifications based on the SF700 anomaly fields can be linked to wetter and drier conditions within the main monsoon period and can therefore

explain a substantial part of the daily rainfall variability during this period.

4.3 | Evaluation of the two-step classification procedure for heavy rainfall

The subseasonal classification was performed for the period of the wettest seasonal CPs, that is, CP2, CP4 and CP5 using MSL, and is used to classify these CPs into subgroups. Since the best subseasonal classification is based on six CPs (see Figure 11), the final classification leads to 23 CPs. The occurrence frequency of the CPs and their precipitation statistics are listed in Table 6. In addition, the number of extremes is shown for each CP, based on the 100 largest precipitation events. The results exhibit a clear discrimination between dry and wet CPs. There are four CPs (CP2.4, CP2.6, CP4.4 and CP4.6) with a clearly increased WI ($WI > 3.5$) compared with the wettest CP of the seasonal classification (CP4, $WI = 3.26$). The two wettest subclasses (i.e., CP4.4 and CP4.6) caused 45% of the extremes, although they occurred on only 6.5% of days. Moreover, the six wettest CPs are also responsible for more than 65% of the annual rainfall amount and 63% of the extremes, although these CPs only occur on 11.5% of days. There is also a clear variation of the WI for the different subclasses of CP2, CP4 and CP5. For example, CP4.2 has a WI value of 1.68, compared with 4.5 for CP4.4. Thus, the analysis shows that the final classification can distinguish relatively well between dry and wet CPs during the season and within

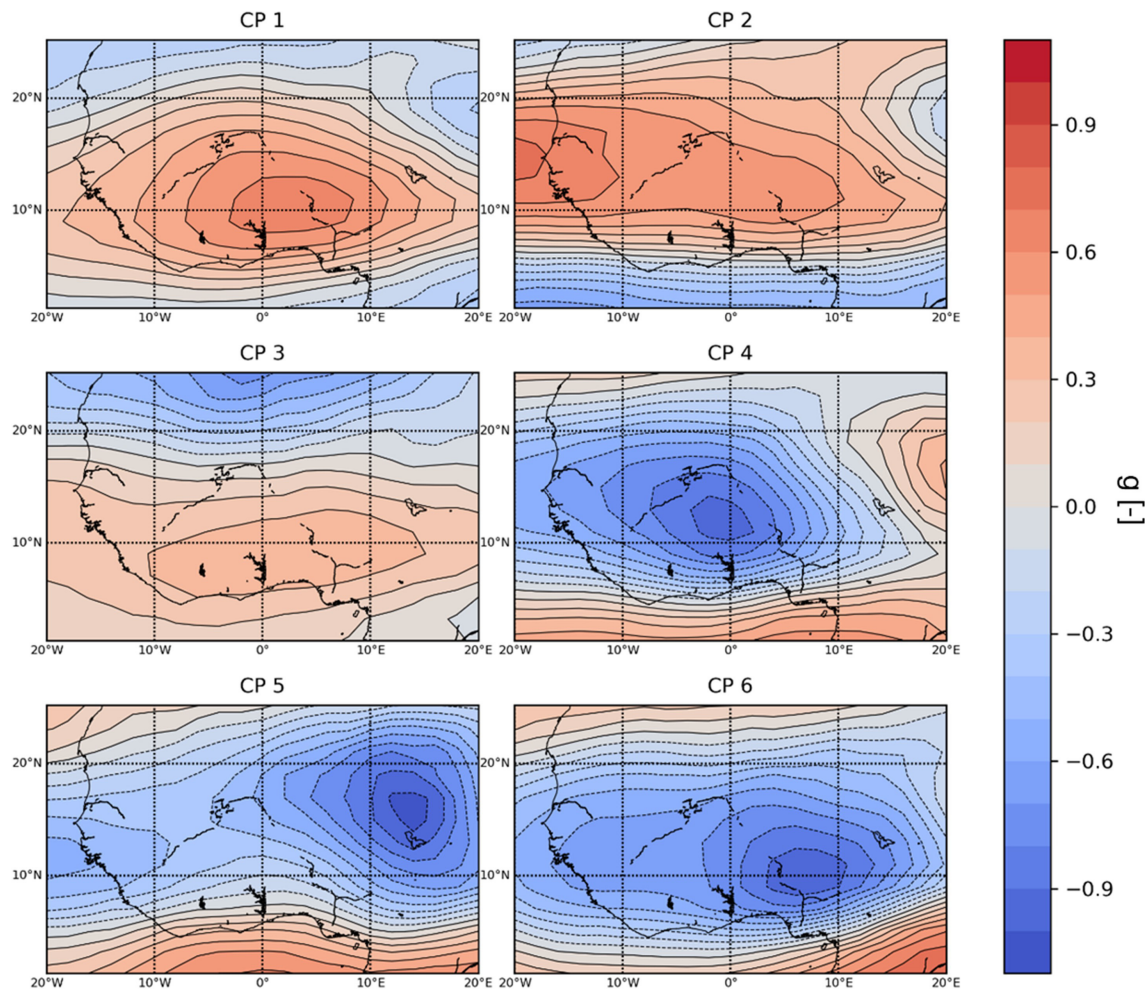


FIGURE 11 Atmospheric circulation patterns (CP) of the stream function anomalies at 700 hPa level within domain B, 1989 to 2010 [Colour figure can be viewed at wileyonlinelibrary.com]

TABLE 5 Circulation pattern (CP) statistics for stream function at 700 hPa within domain B

CP	Occurrence (%)	MDARP (-)	MDARA (mm)	WI (-)
1	27.61	0.22	3.45	0.69
2	17.43	0.20	2.85	0.57
3	16.55	0.26	4.16	0.83
4	15.11	0.45	8.27	1.65
5	5.74	0.27	4.59	0.92
6	17.57	0.42	7.71	1.54

Abbreviations: MDARP, mean daily areal rainfall probability; MDARS, mean daily areal rainfall amount; WI, wetness index.

the monsoon period, and that certain subclasses can be clearly linked to precipitation extremes.

5 | DISCUSSION

The FRBCM is widely applied in Central Europe (e.g., Bárdossy and Filiz, 2005; Wetterhall et al., 2008;

Bárdossy and Pegram, 2011; Rau et al., 2020), but only rarely used in the context of monsoonal areas (e.g., Zehe et al., 2006b; Laux, 2009). In the West African domain, Guèye et al. (2011, 2012) and Moron et al. (2008a) used other well-known classification techniques based on self-organizing maps and k-means cluster analysis. Compared with those existing classifications studies for the WAM region, the advantage of the proposed two-step

CP	Occurrence (%)	MDARP (-)	MDARA (mm)	WI (-)	N_{ex} (-)
1	13.37	0.04	0.39	0.19	0
2.1	2.63	0.16	2.32	1.14	1
2.2	1.84	0.17	2.26	1.11	1
2.3	1.72	0.20	2.93	1.44	2
2.4	0.51	0.39	6.38	3.14	2
2.5	0.25	0.18	1.97	0.97	0
2.6	0.50	0.45	7.67	3.78	1
3	7.37	0.09	1.15	0.57	1
4.1	2.89	0.27	4.52	2.23	7
4.2	1.59	0.24	3.42	1.68	0
4.3	2.04	0.34	5.69	2.80	6
4.4	3.02	0.47	9.13	4.50	21
4.5	0.92	0.29	5.55	2.74	5
4.6	3.53	0.44	8.46	4.17	24
5.1	4.24	0.23	3.44	1.69	2
5.2	2.73	0.20	2.91	1.43	4
5.3	2.09	0.24	3.67	1.81	3
5.4	1.80	0.43	7.39	3.64	6
5.5	0.86	0.26	4.33	2.13	1
5.6	2.18	0.37	6.49	3.20	9
6	22.39	0.01	0.07	0.04	1
7	13.14	0.01	0.07	0.04	0
8	8.39	0.09	1.16	0.57	3

Abbreviations: N_{ex} , Number of extremes based on the 100 wettest days ($>19.6 \text{ mm/d}$); MDARP, mean daily areal rainfall probability; MDARS, mean daily areal rainfall amount; WI, wetness index, 1989–2010.

classification procedure is the second step of the classification, which can be easily adapted in terms of the spatial and temporal domain. This nesting procedure, based on large-scale atmospheric circulation patterns, allows the definition of a dynamic temporal domain for further refinement of the downscaling process, and gives better flexibility to address specific questions, such as determining the onset or cessation of the rainy season for agriculture. A direct comparison between the different studies, however, remains difficult, since the studies differ not only in their specific settings (e.g., spatial domain, period, study area), but also in the methods and metrics to evaluate performance. Thus, a performance comparison between the different approaches is out of the scope of this study.

Despite the different classification techniques, the predictor screening in this study revealed similar results such as Guèye et al. (2011, 2012). They used MSL and the wind fields at 825 hPa, which are closely related to the best-performing predictor variables applied in our final setup for the two-step approach (i.e., MSL and SF700). In

TABLE 6 CP statistics from the joint classification using the two-step procedure based on stream function at 700 hPa and mean sea level pressure

the seasonal classification (step 1), the identified best predictor variables (U1000, V1000, MSL, U700, U200, V850, MFV1000 and GPH1000) are physically related to large-scale WAM processes like SHL, TEJ and the AEJ. This indicates that the classification can describe the seasonal variability in this region, which is a necessary condition for prediction.

Beside the identification of suitable predictor variables, the number of classes (i.e., CPs) and the number of grid points relevant for the fuzzy rules is a crucial but subjective decision in the classification. This has been extensively analysed in this study. Considering the tradeoffs between performance gains during the calibration process and performance losses during validation, eight classes are determined as a good solution for the seasonal classification. This finding is consistent with previous studies for example, Guèye et al. (2011, 2012). Moreover, we showed that the number of grid points relevant for fuzzy rules is a crucial parameter in FRBCM and has a strong impact on classification performance and the transferability of the optimized classification to

an independent dataset. We determined that only a very small portion of the grid points (4%) are relevant for both classification steps. This reduces overfitting of FRBCM and improves classification performance and transferability of the approach to an independent dataset. Our outcome also confirms the information of Zehe et al. (2006b), which used only small portion of grid points (10–12) in their classification for India.

Since the seasonal rainfall component of the WAM is the dominant signal, the discriminatory power of the classification for day-to-day variability of rainfall is expected to be poorer in comparison to seasonal variability. This expectation is confirmed by the results obtained from the subseasonal classification (step 2). It is found that information gain is reduced by about one order of magnitude compared with the seasonal classification. Based on the predictor screening, we identified SF700 as the predictor with the highest information gain. Stream functions are used in order to objectively identify AEW trough axes and AEJ axes, as shown by Berry et al. (2007). To the best of our knowledge, no further study has applied a stream function field for the CP classification in West Africa. Based on the wettest classes obtained from the seasonal classification, the subseasonal classification identified suitable subclasses to describe extreme rainfall events, that is, classes with WI values remarkably different from 1. We cross-checked the time series of the CP catalogue with observed extreme rainfall events in Burkina Faso. As an example, the extremely severe heavy rainfall event on September first, 2009, in Ouagadougou (Engel et al., 2017) is grouped within CP4.6, one of the wettest patterns in our approach. This CP type is characterized by an intensified SHL pattern (CP4 in Figure 8) and a cyclonic rotation over the study area (CP6 in Figure 11), indicating an AEW trough. This situation is known as a favourable condition for generating rain-producing systems. However, AEW are not the only type of atmospheric wave influencing the daily rainfall variability in this region (Schlueter et al., 2019a). Lafore et al. (2017) showed that a simultaneous occurrence of a convectively coupled Kelvin wave and equatorial Rossby wave played a strong role for the heavy rainfall event in Ouagadougou, 1 September 2009. Moreover, the CPs shown in Figure 11 indicate a larger wavelength in comparison to a typical wavelength of AEW waves (~ 2500 km, Diedhiou et al., 1998). Thus, the current CPs can be also mixture of different wave types for this region. To explore this issue in more detail, a more rigorous process-based analysis of the determined atmospheric patterns is needed in future investigations. This is shown for classification approaches by Moron et al. (2008a) and Guèye et al. (2011, 2012) for this region.

The seasonal CP patterns are also consistent with Lavaysse et al. (2009) to a large degree. They pointed out

that the average heat low position during the dry phase is at 8.9°N , 14.3°E (standard deviation of 2.44° and 5.9° , respectively) and at 23.8°N , 0°E (standard deviation of 2.2° and 4.1° , respectively) for the wet phase. This is relatively in line with our summer phase CPs (CP2, CP4 and CP5) and the dry phase CPs (in particular CP7). Moreover, the identified CPs of the subseasonal classification, associated with intense rainfall amounts (CP4 and CP6), are related to westward propagating wind systems at 700 hPa. This is in agreement with the study by Camberlin et al. (2020). Thus, the classification can generate relatively reliable CP patterns for the study region of interest. Nevertheless, the determined CPs of the seasonal classification are relatively similar compared with the spatial patterns of a straightforward monthly classification due to the strong overlying seasonal variation of this region. However, a monthly classification does not allow any flexibility in terms of late or early monsoon and a classification based on atmospheric variables should be therefore preferred.

The classification still offers potential for improvement. Moron et al. (2008a) included more predictor variables in the classification process, such as the wind fields at 200, 700 and 925 hPa. Lavaysse et al. (2009) used the thickness of the geopotential height for describing the transition of the West African heat low. A comprehensive predictor study was also done by Deme et al. (2003) for the prediction of daily rainfall in Senegal. Based on this investigation, other variables that were not used in this study are also relevant for daily rainfall, like the lifting condensation level. Another important setting is the predictor domain used in downscaling (Wetterhall et al., 2006; Radanovics et al., 2013). Wetterhall et al. (2007) illustrated that the domain of the FRBCM has an influence and can therefore improve the downscaling process. Moreover, the selected predictor time step (12 UTC) might be not the best choice since midday local forcings are the strongest and can therefore perturb the large-scale circulation. Thus, other time steps might be relevant, too. For instance, Guèye et al. (2012) selected 0, 6 and 18 UTC for the classification, as well. In addition, several other processes that influence rainfall variability in West Africa are not yet considered. For instance, the Madden–Julian Oscillation is known to be relevant for the rainfall variability on timescales between 30 and 90 days (Schlueter, 2020) and SST patterns and ENSO can have an influence on the interannual rainfall variability (Nicholson, 2013).

6 | CONCLUSIONS

In this study, a two-step atmospheric circulation pattern classification consisting of a seasonal and a subseasonal

classification was developed for West Africa to describe the seasonal and day-to-day variability of rainfall in the Sudan-Sahel zone.

In the seasonal classification, the best performing predictor variables (e.g., surface pressure, meridional moisture fluxes) for describing the seasonal rainfall variability are closely related to the main governing atmospheric processes of the WAM (e.g., SHL, TEJ and the AEJ), giving evidence for the reliability of ERA5 reanalysis data and the chosen classification approach. In the subseasonal classification, the stream function at 700 hPa as an indicator for troughs and ridges of tropical waves shows the highest performance in describing daily rainfall variability during the monsoon period. It is concluded that the subseasonal classification adds additional value to the overall performance of the classification. The new approach can therefore better separate between dry and wet CPs in the study region. Moreover, specific subclasses of wet CPs could be linked to synoptic situations, responsible for 85% of the extremes, of which only two caused nearly half of the extremes on 6.5% of the days. These CPs are characterized by an intensified SHL and evidence of a cyclonic rotation close to the study region in Burkina Faso, indicating a wave trough in this region.

A crucial parameter for the chosen classification approach is the number of grid points relevant for the fuzzy rules. We discovered that a relatively small number of grid points within the predictor domain is sufficient for this classification. This reduces overfitting and therefore enhances overall model performance and transferability to an independent dataset.

The presented CP classification opens many different possibilities for statistical applications in climate sciences and other disciplines in the WAM region. The CP classification can be used to improve state-of-the-art stochastic approaches used for rainfall simulation in this region (e.g., Vischel et al., 2009; Wilcox et al., 2021) by conditioning the rainfall statistics to the CP-type (e.g., Stehlík and Bárdossy, 2002; Zehe et al., 2006b). Moreover, CP classifications can be also applied as conditional information in downscaling (Haberlandt et al., 2015), to improve common approaches used for climate projections or seasonal forecasting (e.g., Siegmund et al., 2015; Rauch et al., 2019), to better predict rainfall and other meteorological variables in this challenging region.

ACKNOWLEDGEMENTS

This study was part of WASCAL (West African Science Service Centre on Climate Change and Adapted Land Use), SAWAM (Seasonal Water Management for Semi-arid Areas) and the ENERSHELF (Energy-Self-Sufficiency for Health Facilities in Ghana) project. The projects are granted by the

Federal Ministry of Education and Research in Germany (WASCAL grant number: 01LG1202C1, SAWAM grant number: 02WGR1421 and ENERSHELF grant number: 03SF0567D). We also want to acknowledge the meteorological service of Burkina Faso ANAM (*Agence National de la Météorologie—Burkina Faso*) who provided the precipitation data as part of the WASCAL program. Finally, we also want to thank two anonymous reviewers for their valuable comments and suggestions for improvement.

AUTHOR CONTRIBUTIONS

Jan Bliefernicht: Conceptualization; investigation; methodology; supervision; writing – original draft; writing – review and editing. **Manuel Rauch:** Formal analysis; investigation; methodology; software; visualization; writing – original draft. **Patrick Laux:** Supervision; writing – original draft; writing – review and editing. **Harald Kunstmann:** Funding acquisition; supervision; writing – review and editing.

ORCID

Jan Bliefernicht  <https://orcid.org/0000-0002-8591-6231>
 Patrick Laux  <https://orcid.org/0000-0002-8657-6152>
 Harald Kunstmann  <https://orcid.org/0000-0001-9573-1743>

REFERENCES

- Ascott, M.J., et al. (2020) In situ observations and lumped parameter model reconstructions reveal intra-annual to multidecadal variability in groundwater levels in sub-Saharan Africa. *Water Resources Research*, 56(12), e2020WR028056. <https://doi.org/10.1029/2020WR028056>.
- Bárdossy, A. (2010) Atmospheric circulation pattern classification for south-West Germany using hydrological variables. *Physics and Chemistry of the Earth*, 35(9–12), 498–506. <https://doi.org/10.1016/j.pce.2010.02.007>.
- Bárdossy, A. and Filiz, F. (2005) Identification of flood producing atmospheric circulation patterns. *Journal of Hydrology*, 313(1–2), 48–57.
- Bárdossy, A., L., D. and Borgardi, I. (1995) Fuzzy rule-based classification of atmospheric circulation patterns. *International Journal of Climatology*, 15(10), 1087–1097.
- Bárdossy, A. and Pegram, G. (2011) Downscaling precipitation using regional climate models and circulation patterns toward hydrology. *Water Resources Research*, 47(4), 1–18. <https://doi.org/10.1029/2010WR009689>.
- Bárdossy, A., Stehlík, J. and Caspary, H.J. (2002) Automated objective classification of daily circulation patterns for precipitation and temperature downscaling based on optimized fuzzy rules. *Climate Research*, 23(1), 11–22.
- Berry, G., Thorncroft, C. and Hewson, T. (2007) African easterly waves during 2004: analysis using objective techniques. *Monthly Weather Review*, 135(4), 1251–1267. <https://doi.org/10.1175/MWR3343.1>.

- Bifieernicht, J. (2010) Probability Forecasts of Daily Areal Precipitation for Small River Basins. PhD thesis, Mitteilungen, Institut für Wasserbau, Universität Stuttgart, 194, pp. 167. <https://doi.org/10.18419/opus-361>.
- Bifieernicht, J., et al. (2018) The WASCAL hydrometeorological observatory in the Sudan Savanna of Burkina Faso and Ghana. *Vadose Zone Journal*, 17(1), 1–20. <https://doi.org/10.2136/vzj2018.03.0065>.
- Bifieernicht, J., et al. (2019) Quality and value of seasonal precipitation forecasts issued by the West African regional climate outlook forum. *Journal of Applied Meteorology and Climatology*, 58 (3), 621–642. <https://doi.org/10.1175/JAMC-D-18-0066.1>.
- Bifieernicht, J., et al. (2021) Towards a historical precipitation database for West Africa: overview, quality control and harmonization. *International Journal of Climatology*, 1–23. <https://doi.org/10.1002/joc.7467>.
- Bifieernicht, J. and Bárdossy, A. (2007) Probabilistic forecast of daily areal precipitation focusing on extreme events. *Natural Hazards and Earth System Science*, 7(2), 263–269. <https://doi.org/10.5194/nhess-7-263-2007>.
- Brammer, A. and Thorncroft, C.D. (2015) Variability and evolution of African easterly wave structures and their relationship with tropical cyclogenesis over the eastern Atlantic. *Monthly Weather Review*, 143(12), 4975–4995. <https://doi.org/10.1175/MWR-D-15-0106.1>.
- Brands, S., et al. (2012) On the use of reanalysis data for downscaling. *Journal of Climate*, 25(7), 2517–2526. <https://doi.org/10.1175/JCLI-D-11-00251.1>.
- Camberlin, P., Kpanou, M. and Roucou, P. (2020) Classification of intense rainfall days in southern West Africa and associated atmospheric circulation. *Atmosphere*, 1–26. <https://doi.org/10.3390/atmos11020188>.
- Chernick, M.R. (2011) *Bootstrap methods: A guide for practitioners and researchers*. Hoboken, NJ: John Wiley & Sons.
- Dai, A., et al. (2004) The recent Sahel drought is real. *International Journal of Climatology*, 24(11), 1323–1331. <https://doi.org/10.1002/joc.1083>.
- Dee, D.P., et al. (2011) The ERA-Interim reanalysis: configuration and performance of the data assimilation system. *Quarterly Journal of the Royal Meteorological Society*, 137(656), 553–597. <https://doi.org/10.1002/qj.828>.
- Deme, A., Viltard, A. and de Félice, P. (2003) Daily precipitation forecasting in Dakar using the NCEP–NCAR reanalyses. *Weather and Forecasting*, 18(1), 93–105. [https://doi.org/10.1175/1520-0434\(2003\)018<0093:DPFIDU>2.0.CO;2](https://doi.org/10.1175/1520-0434(2003)018<0093:DPFIDU>2.0.CO;2).
- Diedhiou, A., et al. (1998) Evidence of two regimes of easterly waves over West Africa and the tropical Atlantic. *Geophysical Research Letters*, 25(15), 2805–2808. <https://doi.org/10.1029/98GL02152>.
- Dieng, D., et al. (2017) Evaluation of the COSMO-CLM high-resolution climate simulations over West Africa. *Journal of Geophysical Research*, 122(3), 1437–1455. <https://doi.org/10.1002/2016JD025457>.
- Dieng, D., et al. (2018) Performance analysis and projected changes of agroclimatological indices across West Africa based on high-resolution regional climate model simulations. *Journal of Geophysical Research: Atmospheres*, 123(15), 7950–7973. <https://doi.org/10.1029/2018JD028536>.
- Efron, B. and Tibshirani, R.J. (1994) *An introduction to the bootstrap*. Boca Raton, FL: CRC Press.
- EM-DAT (2020) The international disaster database. <https://www.cred.be/index.php?q=projects/EM-DAT>
- Engel, T., et al. (2017) Extreme precipitation in the west African cities of Dakar and Ouagadougou: atmospheric dynamics and implications for flood risk assessments. *Journal of Hydrometeorology*, 18(11), 2937–2957. <https://doi.org/10.1175/JHM-D-16-0218.1>.
- Fink, A.H. and Reiner, A. (2003) Spatiotemporal variability of the relation between African easterly waves and west African squall lines in 1998 and 1999. *Journal of Geophysical Research: Atmospheres*, 108(D11), 1–17. <https://doi.org/10.1029/2002JD002816>.
- Giorgi, F. and Gutowski, W.J. (2015) Regional dynamical downscaling and the CORDEX initiative. *Annual Review of Environment and Resources*, 40(1), 467–490. <https://doi.org/10.1146/annurev-environ-102014-021217>.
- Guèye, A.K., et al. (2011) Weather regimes over Senegal during the summer monsoon season using self-organizing maps and hierarchical ascendant classification. Part I: synoptic time scale. *Climate Dynamics*, 36(1), 1–18. <https://doi.org/10.1007/s00382-010-0782-6>.
- Guèye, A.K., et al. (2012) Weather regimes over Senegal during the summer monsoon season using self-organizing maps and hierarchical ascendant classification. Part II: interannual time scale. *Climate Dynamics*, 39(9), 2251–2272. <https://doi.org/10.1007/s00382-012-1346-8>.
- Haberlandt, U., Belli, A. and Bárdossy, A. (2015) Statistical downscaling of precipitation using a stochastic rainfall model conditioned on circulation patterns: an evaluation of assumptions. *International Journal of Climatology*, 35(3), 417–432. <https://doi.org/10.1002/joc.3989>.
- Heinzel, D., et al. (2018) The WASCAL high-resolution regional climate simulation ensemble for West Africa: concept, dissemination and assessment. *Earth System Science Data*, 10(2), 815–835. <https://doi.org/10.5194/essd-10-815-2018>.
- Hersbach, H., et al. (2019) Global reanalysis: goodbye ERA-Interim, hello ERA5. *ECMWF Newsletter*, 159, 17–24. <https://doi.org/10.21957/vf291hehd7>.
- Hersbach, H., et al. (2020) The ERA5 global reanalysis. *Quarterly Journal of the Royal Meteorological Society*, 146(730), 1999–2049. <https://doi.org/10.1002/qj.3803>.
- Hewitson, B.C., et al. (2014) Interrogating empirical-statistical downscaling. *Climatic Change*, 122(4), 539–554. <https://doi.org/10.1007/s10584-013-1021-z>.
- Huth, R., et al. (2008) Classifications of atmospheric circulation patterns. *Annals of the New York Academy of Sciences*, 1146(1), 105–152. <https://doi.org/10.1196/annals.1446.019>.
- Lafore, J.-P., et al. (2017) A multi-scale analysis of the extreme rain event of Ouagadougou in 2009. *Quarterly Journal of the Royal Meteorological Society*, 143(709), 3094–3109. <https://doi.org/10.1002/qj.3165>.
- Laux, P., et al. (2009) Modelling daily precipitation features in the Volta Basin of West Africa. *International Journal of Climatology*, 29(7), 937–954. <https://doi.org/10.1002/joc.1852>.
- Laux, P. (2009) Statistical modeling of precipitation for agricultural planning in the Volta Basin of West Africa. *Mitteilungen des*

- Instituts für Wasser- und Umweltsystemmodellierung. University of Stuttgart. <https://doi.org/10.18419/opus-303>.
- Laux, P., Kunstmann, H. and Bárdossy, A. (2008) Predicting the regional onset of the rainy season in West Africa. *International Journal of Climatology*, 28(3), 329–342. <https://doi.org/10.1002/joc.1542>.
- Lavaysse, C., et al. (2009) Seasonal evolution of the West African heat low: a climatological perspective. *Climate Dynamics*, 33(2), 313–330. <https://doi.org/10.1007/s00382-009-0553-4>.
- Li, X. and Claramunt, C. (2006) A spatial entropy-based decision tree for classification of geographical information. *Transactions in GIS*, 10(3), 451–467. <https://doi.org/10.1111/j.1467-9671.2006.01006.x>.
- Li, Z., Chao, Y. and McWilliams, J.C. (2006) Computation of the streamfunction and velocity potential for limited and irregular domains. *Monthly Weather Review*, 134(11), 3384–3394. <https://doi.org/10.1175/MWR3249.1>.
- Maraun, D. and Widmann, M. (2018) *Statistical downscaling and bias correction for climate research*. Cambridge: Cambridge University Press. <https://doi.org/10.1017/9781107588783>.
- Markantonis, V., et al. (2018) Assessing floods and droughts in the Mékrou River basin (West Africa): a combined household survey and climatic trends analysis approach. *Natural Hazards and Earth System Sciences*, 18(4), 1279–1296. <https://doi.org/10.5194/nhess-18-1279-2018>.
- Moron, V., et al. (2008a) Weather types and rainfall over Senegal. Part I: observational analysis. *Journal of Climate*, 21(2), 266–287. <https://doi.org/10.1175/2007JCLI1601.1>.
- Moron, V., et al. (2008b) Weather types and rainfall over Senegal. Part II: downscaling of GCM simulations. *Journal of Climate*, 21(2), 288–307. <https://doi.org/10.1175/2007JCLI1624.1>.
- Moron, V., et al. (2018) Daily weather types in February–June (1979–2016) and temperature variations in tropical North Africa. *Journal of Applied Meteorology and Climatology*, 57(5), 1171–1195. <https://doi.org/10.1175/JAMC-D-17-0105.1>.
- Munich RE (2019) Data on natural disasters since 1980. <https://www.munichre.com/en/solutions/reinsurance-property-casualty/natcatservice.html>
- Nicholson, S.E. (2001) Climatic and environmental change in Africa during the last two centuries. *Climate Research*, 17, 123–144. <https://doi.org/10.3354/cr017123>.
- Nicholson, S.E. (2013) The west African Sahel: a review of recent studies on the rainfall regime and its interannual variability. *ISRN Meteorology*, 2013, 1–32. <https://doi.org/10.1155/2013/453521>.
- Nicholson, S.E., Funk, C. and Fink, A.H. (2018) Rainfall over the African continent from the 19th through the 21st century. *Global and Planetary Change*, 165, 114–127. <https://doi.org/10.1016/j.gloplacha.2017.12.014>.
- Philipp, A., et al. (2016) Development and comparison of circulation type classifications using the COST 733 dataset and software. *International Journal of Climatology*, 36(7), 2673–2691. <https://doi.org/10.1002/joc.3920>.
- Pringle, J., Stretch, D.D. and Bárdossy, A. (2015) On linking atmospheric circulation patterns to extreme wave events for coastal vulnerability assessments. *Natural Hazards*, 79(1), 45–59. <https://doi.org/10.1007/s11069-015-1825-4>.
- Quinlan, J.R. (1986) Induction of decision trees. *Machine Learning*, 1(1), 81–106. <https://doi.org/10.1007/BF00116251>.
- Radanovics, S., et al. (2013) Optimising predictor domains for spatially coherent precipitation downscaling. *Hydrology and Earth System Sciences*, 17(10), 4189–4208. <https://doi.org/10.5194/hess-17-4189-2013>.
- Rau, M., et al. (2020) Statistical downscaling to project extreme hourly precipitation over the United Kingdom. *International Journal of Climatology*, 40(3), 1805–1823. <https://doi.org/10.1002/joc.6302>.
- Rauch, M., et al. (2019) Seasonal forecasting of the onset of the rainy season in West Africa. *Atmosphere*, 1–21. <https://doi.org/10.3390/atmos10090528>.
- Reed, R. J., Norquist, D. C. and Recker, E. E. (1977) The structure and properties of African wave disturbances as observed during phase III of GATE. *Monthly Weather Review*, 105, 317–333.
- Salack, S., et al. (2016) Global warming induced hybrid rainy seasons in the Sahel. *Environmental Research Letters*, 11(10), 1–11. <https://doi.org/10.1088/1748-9326/11/10/104008>.
- Schlüter, A., et al. (2019a) A systematic comparison of tropical waves over northern Africa. Part I: influence on rainfall. *Journal of Climate*, 32(5), 1501–1523. <https://doi.org/10.1175/JCLI-D-18-0173.1>.
- Schlüter, A. (2020) *Synoptic to intraseasonal variability of African rainfall*. Oxford: Oxford University Press. <https://doi.org/10.1093/acrefore/9780190228620.013.522>.
- Schlüter, A., Fink, A.H. and Knippertz, P. (2019b) A systematic comparison of tropical waves over northern Africa. Part II: dynamics and thermodynamics. *Journal of Climate*, 32(9), 2605–2625. <https://doi.org/10.1175/JCLI-D-18-0651.1>.
- Shannon, C.E. (1948) A mathematical theory of communication. *The Bell System Technical Journal*, 27(3), 379–423. <https://doi.org/10.1002/j.1538-7305.1948.tb01338.x>.
- Siegmund, J., et al. (2015) Toward a seasonal precipitation prediction system for West Africa: performance of CFSv2 and high-resolution dynamical downscaling. *Journal of Geophysical Research*, 120(5), 7316–7339. <https://doi.org/10.1002/2014JD022692>.
- Smith, D.M., Scaife, A.A. and Kirtman, B.P. (2012) What is the current state of scientific knowledge with regard to seasonal and decadal forecasting? *Environmental Research Letters*, 7(1), 15602. <https://doi.org/10.1088/1748-9326/7/1/015602>.
- Stehlik, J. and Bárdossy, A. (2002) Multivariate stochastic downscaling model for generating daily precipitation series based on atmospheric circulation. *Journal of Hydrology*, 256(1–2), 120–141.
- Taylor, C.M., et al. (2017) Frequency of extreme Sahelian storms tripled since 1982 in satellite observations. *Nature*, 544(7651), 475–478. <https://doi.org/10.1038/nature22069>.
- Tazen, F., et al. (2019) Trends in flood events and their relationship to extreme rainfall in an urban area of Sahelian West Africa: the case study of Ouagadougou, Burkina Faso. *Journal of Flood Risk Management*, 12(S1), e12507. <https://doi.org/10.1111/jfr3.12507>.
- UN (2020) World Population Prospects 2019. <https://population.un.org/wpp/Download/Standard/Population/>.
- Vischel, T., et al. (2009) Conditional simulation schemes of rain fields and their application to rainfall-runoff modeling studies in the Sahel. *Journal of Hydrology*, 375(1), 273–286. <https://doi.org/10.1016/j.jhydrol.2009.02.028>.

- Vogel, P., et al. (2018) Skill of global raw and postprocessed ensemble predictions of rainfall over northern tropical Africa. *Weather and Forecasting*, 33(2), 369–388. <https://doi.org/10.1175/WAF-D-17-0127.1>.
- Wetterhall, F., et al. (2006) Daily precipitation-downscaling techniques in three Chinese regions. *Water Resources Research*, 42 (11), 1–13. <https://doi.org/10.1029/2005WR004573>.
- Wetterhall, F., et al. (2008) Statistical downscaling of daily precipitation over Sweden using GCM output. *Theoretical and Applied Climatology*, 96(1), 95. <https://doi.org/10.1007/s00704-008-0038-0>.
- Wetterhall, F., Halldin, S. and Xu, C.-Y. (2007) Seasonality properties of four statistical-downscaling methods in Central Sweden. *Theoretical and Applied Climatology*, 87(1), 123–137. <https://doi.org/10.1007/s00704-005-0223-3>.
- Wilcox, C., et al. (2021) Stochastorm: a stochastic rainfall simulator for convective storms. *Journal of Hydrometeorology*, 22(2), 387–404. <https://doi.org/10.1175/JHM-D-20-0017.1>.
- Wilks, D.S. (2011) *Statistical methods in the atmospheric sciences*. Amsterdam: Academic Press.
- Zehe, E., Singh, A.K. and Bárdossy, A. (2006a) Modelling of monsoon rainfall for a mesoscale catchment in north-West India I: assessment of objective circulation patterns. *Hydrology and Earth System Sciences*, 10(6), 797–806. <https://doi.org/10.5194/hess-10-797-2006>.
- Zehe, E., Singh, A.K. and Bárdossy, A. (2006b) Modelling of monsoon rainfall for a mesoscale catchment in north-West India II: stochastic rainfall simulations. *Hydrology and Earth System Sciences*, 10(6), 807–815. <https://doi.org/10.5194/hess-10-807-2006>.

How to cite this article: Bliefernicht, J., Rauch, M., Laux, P., & Kunstmann, H. (2022).

Atmospheric circulation patterns that trigger heavy rainfall in West Africa. *International Journal of Climatology*, 42(12), 6515–6536. <https://doi.org/10.1002/joc.7613>

APPENDIX A

SIMULATED ANNEALING ALGORITHM

The basis for the optimization algorithm of the fuzzy rule-based classification is a simulated annealing approach. This algorithm is described by Bárdossy et al. (2002). However, the model parameter ANC is not listed in this reference. This information was given in the FORTRAN code provided by András Bárdossy in former investigations (e.g., Laux, 2009). In this study, we used the information given in the different references of the fuzzy approach and the FORTRAN code and recoded the approach in Python. The different steps of the simulated annealing algorithm used in this study can be therefore described as follows:

1. Set initial annealing temperature q_0
2. Select rule k randomly
3. Select location i randomly
4. Select a class v^* randomly
5. Evaluate several requirements to continue:
 - a. The allowed number of classes (ANC) (classes 1–4) for the description of a CP is not higher than a specified threshold
 - b. The ANC is not lower than a specified threshold
 - c. $v(i,k)$ is unequal to v^*
 - d. The absolute difference to neighbour grid points classes is not higher than 1
 - e. If these conditions are not fulfilled repeat step 2, otherwise continue with step 6

1. Set $v(i,k)=v^*$ and execute the classification
2. Calculate O^* for new rules
3. If $O^* > O$, accept the change
4. If $O^* \leq O$:
 - a. Generate a random number z between 0 and 1
 - b. If $z < \exp\left(-\frac{O-O^*}{q_s}\right)$, accept the change, else keep the existing classification
5. Repeat steps 2 to 9 M times
6. Decrease the annealing temperature
7. Repeat steps 2 to 11 until the changes are below a certain threshold (number of changes $< M/100$).

The initial annealing temperature q_0 is set to 50 and the iteration number M to 1000.